

Complete Structure of the 11-Subunit Bovine Mitochondrial Cytochrome bc_1 Complex

So Iwata,* Joong W. Lee, Kengo Okada,† John Kyongwon Lee, Momi Iwata, Bjarne Rasmussen, Thomas A. Link, S. Ramaswamy, Bing K. Jap*

Mitochondrial cytochrome bc_1 complex performs two functions: It is a respiratory multienzyme complex and it recognizes a mitochondrial targeting presequence. Refined crystal structures of the 11-subunit bc_1 complex from bovine heart reveal full views of this bifunctional enzyme. The "Rieske" iron-sulfur protein subunit shows significant conformational changes in different crystal forms, suggesting a new electron transport mechanism of the enzyme. The mitochondrial targeting presequence of the "Rieske" protein (subunit 9) is lodged between the two "core" subunits at the matrix side of the complex. These "core" subunits are related to the matrix processing peptidase, and the structure unveils how mitochondrial targeting presequences are recognized.

Cytochrome bc_1 complex (otherwise known as complex III of the respiratory chain or ubiquinol:cytochrome c oxidoreductase) is an oligomeric electron transfer enzyme complex found in the inner mitochondrial membrane of eukaryotes and in the plasma membrane of bacteria (1, 2). This complex is the middle component of the mitochondrial respiratory chain, coupling the transfer of electrons from ubihydroquinone to cytochrome c with the generation of a proton gradient across the mitochondrial membrane. Every bc_1 complex contains three common subunits with active redox centers {cytochrome b, cytochrome c_1 , and the "Rieske" [2Fe-2S] protein (ISP)} (3). The mitochondrial system contains additional subunits not present in the bacterial complexes (4, 5).

Bovine heart mitochondrial bc_1 complex

J. W. Lee, J. K. Lee, and B. K. Jap are in the Life Sciences Division, Lawrence Berkeley National Laboratory, University of California, Berkeley, CA 94720, USA. S. Iwata, K. Okada, and M. Iwata are in the Department of Biochemistry, Uppsala University, BMC, Box 576, Uppsala S-75123, Sweden. S. Ramaswamy is in the Department of Molecular Biology, Swedish Agricultural Science University, Box 590, Biomedical Center, Uppsala S-75124, Sweden. T. A. Link is at Uniklinikum Frankfurt, ZBC, Biochemie I, Molecular Bioenergetics, D-60590 Frankfurt/Main, Germany. B. Rasmussen is at the Grenoble Outstation, European Molecular Biology Laboratory, c/o Institut Laue-Langevin, Boîte Postale 156, F-38042 Grenoble Cedex 9, France.

*To whom correspondence should be addressed. E-mail: BKJap@lbl.gov (B.K.J.) or iwata@xray.bmc.uu.se (S.I.)

†Present address: Nara Institute of Science and Technology, Division of Structural Biology, Department of Molecular Biology, Graduate School of Biological Sciences, 8916-5 Takayama, Ikoma, Nara 630-0101, Japan.

is a dimer, with each monomer consisting of 11 different polypeptide subunits; the primary structures of all 11 subunits are known and the total mass of a monomer is ~240 kD. The "core" subunits (subunits 1 and 2) of the bc_1 complex have been shown to be members of the mitochondrial processing peptidase (MPP) family of proteins, suggesting that the bc_1 complex may be a bifunctional protein also involved in mitochondrial import protein processing (6, 7).

There have been recent advances toward the goal of a complete atomic structure of the bc_1 complex. Deisenhofer and Yu's group reported a partial structure of the bc_1 complex from bovine heart mitochondria based on their tetragonal space group crystals (8). In their structure, 5 of the 11 subunits are completely assigned with their amino acid sequences, but the functional domains containing the redox centers of two of the three redox subunits (cytochrome c_1 and the ISP) are essentially missing. Berry and Kim's group recently showed two different locations for the extramembranous domain of the ISP in the chicken bc_1 complex fitted with bovine enzyme sequences (9). They suggested that the ISP may possibly be moving around a pivot joint during the catalytic cycle of the functioning bc_1 complex.

We report the complete atomic resolution structures of the entire 11-subunit bovine heart mitochondrial cytochrome bc_1 complex from crystals belonging to two different space groups, $P6_5$ and $P6_522$, as well as inhibitor-bound complexes (myxothiazol and antimycin A) for the $P6_522$ form.

Structure Determination and Overview. We used two crystal forms ($P6_522$ $a = b =$

211.2 Å, $c = 339.3$ Å; and $P6_5$, $a = b = 130.1$ Å, $c = 720.9$ Å), both of which were obtained from oxidized bovine heart mitochondrial bc_1 complex (10). The asymmetric unit of the $P6_522$ form contains one monomer (composed of 11 subunits) that is related to the other monomer of the dimer by a crystallographic twofold symmetry axis. The asymmetric unit of the $P6_5$ crystals, on the other hand, contains the whole dimer of the bc_1 complex. The maximum diffraction resolution of the $P6_522$ and $P6_5$ crystals are 3.0 and 2.8 Å, respectively. Data collection, structural determination, and crystallographic refinement are summarized in Table 1. The R factors of the models are high compared to ordinary water-soluble protein structures (28.5% for $P6_522$ and 32.0% for $P6_5$) due to partially ordered lipids that are not accounted for in the current model. This unaccounted-for mass represents about 40 to 50 kD in the molecule. In spite of this, a very high quality electron density map for the bc_1 complex has been obtained after refinement, as indicated by the clear electron density around cytochrome c_1 and the ISP in the $P6_522$ form (Fig. 1A).

An overall view of the cytochrome bc_1 complex from the $P6_522$ form viewed parallel to the membrane is presented in Fig. 1B. The intermembrane side of the complex comprises the functional domains of cytochrome c_1 and the ISP, as well as subunit 8. In the transmembrane region, previously unassigned subunits 10 and 11 are assigned, in addition to the four previously known membrane-spanning components (cytochrome b, subunit 7, and the transmembrane helices of the ISP and cytochrome c_1). The matrix side of the bc_1 complex is composed of the large core proteins (subunits 1 and 2), subunit 6, and subunit 9 (the presequence of the ISP), which is located between the two core proteins. The refined structural model of the $P6_522$ crystal contains 2080 residues as follows: SU1 (Core 1), residues 1 to 446; SU2 (Core 2), 21 to 439; SU3 (cytochrome b), 1 to 379; SU4 (cytochrome c_1), 1 to 241; SU5 (ISP), 1 to 196; SU6, 5 to 110; SU7, 1 to 81; SU8, 15 to 78; SU9, 21 to 78; SU10, 1 to 62; and SU11, 17 to 44. Heme b_L , heme b_H , heme c_1 , and the ISP's [2Fe-2S] cluster have been included in the current model. Similar degrees of structural completeness were obtained for the $P6_5$ crystal form as well, except that residues 76 to 196 of the ISP in one monomer show a mixture of at least two different conformational states. The newly assigned subunits are described in the following sections.

Intermembrane Side. General features. Cytochrome c_1 , the ISP, and subunit 8 are positioned on top of cytochrome b (Fig. 2, A and B). The functional domain of cytochrome c_1 is sitting on a horizontal helix α_{ab} (residues 61 to 73) and the first half of loop ef (residues 246 to 261) of cytochrome b. For the $P6_522$ form, the ISP functional domain is

located on top of the other half of loop ef (residues 262 to 268) of cytochrome b and is also associated with cytochrome c_1 . Subunit 8 is in close contact with the NH_2 -terminal extension and loop $\alpha 3$ - $\beta 1$ of cytochrome c_1 , and the COOH-terminal of subunit 7, and furthermore, is predominantly exposed to the solvent. Remarkably, the ISPs are intertwined between the two monomers [that is, the functional domain of the ISP from one monomer interacts with the two redox subunits (cytochrome b and cytochrome c_1) of the other monomer].

"Rieske" [2Fe-2S] protein (ISP). The ISP functional domains are found at different positions for the two crystal forms (Fig. 2, A and B). Different positions of the [2Fe-2S] cluster have also been reported for the $I4_122$ form of the bovine heart bc_1 complex (8), as well as the native and stigmatellin bound forms of the chicken heart complex (9). For the bovine $I4_122$ form, the position was determined by an anomalous difference Fourier map, because the model of the ISP could not be fitted in the observed electron density. After all of these results were evaluated, the positions of the [2Fe-2S] cluster could be categorized into three different positional states (Fig. 2C). In our $P6_522$ structure, the [2Fe-2S]-heme c_1 and [2Fe-2S]-heme b_L distances (measured from the center of the [2Fe-2S] cluster) are 15.5 and 35.5 Å, respectively; this position of the [2Fe-2S] cluster is close to that observed in the native chicken structure. The orientation of the ISP associated with these cluster locations can be designated as the "c₁" position. The most significant difference between these two "c₁" positional states is a hydrogen bond between His¹⁶¹ of the ISP and one of the propionates of heme c_1 , which is present in our $P6_522$ form but is not reported in the chicken structure. In this positional state, electron transfer between the [2Fe-2S] cluster and cytochrome c_1 should be fast. Bovine $I4_122$ form and the chicken heart bc_1 complex in the presence of stigmatellin are categorized as the "b" positional state (Fig. 2C), because these positions are closer to cytochrome b. The [2Fe-2S] position is assumed to be just above the Q_P site (9). In our $P6_5$ structure, the [2Fe-2S]-heme c_1 and [2Fe-2S]-heme b_L distances are 27.5 and 31.0 Å, respectively; this position is distinctly different from the "c₁" positional state, as well as from the "b" positional state (Fig. 2C). In this form, the closest distance between the Q_P site and His¹⁶¹ of the ISP is ~13 Å; therefore, it is impossible to form a hydrogen bond between His¹⁶¹ and a quinone or inhibitor in the Q_P site. We categorize this position as the "intermediate" ("Int") positional state. The details of the conformational change will be discussed below.

Cytochrome c_1 . Cytochrome c_1 is an all- α helix-type protein that resembles other mem-

bers of the cytochrome c family—in particular, Type I cytochrome c (11). The heme ligands are His⁴¹ and Met¹⁶⁰, and the heme is covalently anchored to Cys³⁷ and Cys⁴⁰ (Fig. 2D). One of the heme propionate groups (position 13) forms a salt bridge with Arg¹²⁰. The other propionate (position 17) is free in the $P6_5$ form, whereas it forms a salt bridge with His¹⁶¹ of the ISP in the $P6_522$ form. The subunit is composed of seven helices, including the COOH-terminal membrane helix (with reference to cytochrome c, these are named: $\alpha 1$, residues 23 to 38; $\alpha 1'$, 57 to 73; $\alpha 1''$, 97 to 106; $\alpha 2$, 114 to 119; $\alpha 3$, 123 to 132; $\alpha 5$, 178 to 195; and $\alpha 6$, 197 to 238). The α positions of the 73 residues of the functional domain of cytochrome c_1 can be superimposed onto cytochrome c from horse heart mitochondria (1HRC in Protein Data Bank) with an rms deviation of 1.83 Å. These residues belong mostly to helices $\alpha 1$, $\alpha 2$, $\alpha 3$, and

$\alpha 5$, which surround heme c_1 . There is one distorted double-stranded β -sheet (β -1 and β -2) between helices $\alpha 3$ and $\alpha 5$, in lieu of helix $\alpha 4$ of cytochrome c. Compared to cytochrome c, cytochrome c_1 contains several insertions and deletions between helices. Structural differences appear to be related to specific functions of cytochrome c_1 , including the binding of other subunits as well as soluble cytochrome c. The NH_2 -terminal extension before $\alpha 1$, together with loop $\alpha 3$ - $\beta 1$, form a docking surface for subunit 8. Helix $\alpha 1'$ and loop $\alpha 3$ - $\beta 1$ contain 10 acidic amino acids, many of which point to the intermembrane side and surround the heme c_1 crevice (Fig. 2D). A methyl group at position 12 of heme c_1 as well as its α -cysteinylothioether bond with Cys⁴⁰ from loop $\alpha 1$ - $\alpha 1'$ are exposed to the solvent. This crevice is the most likely binding site of cytochrome c, as indicated by chemical modification experiments

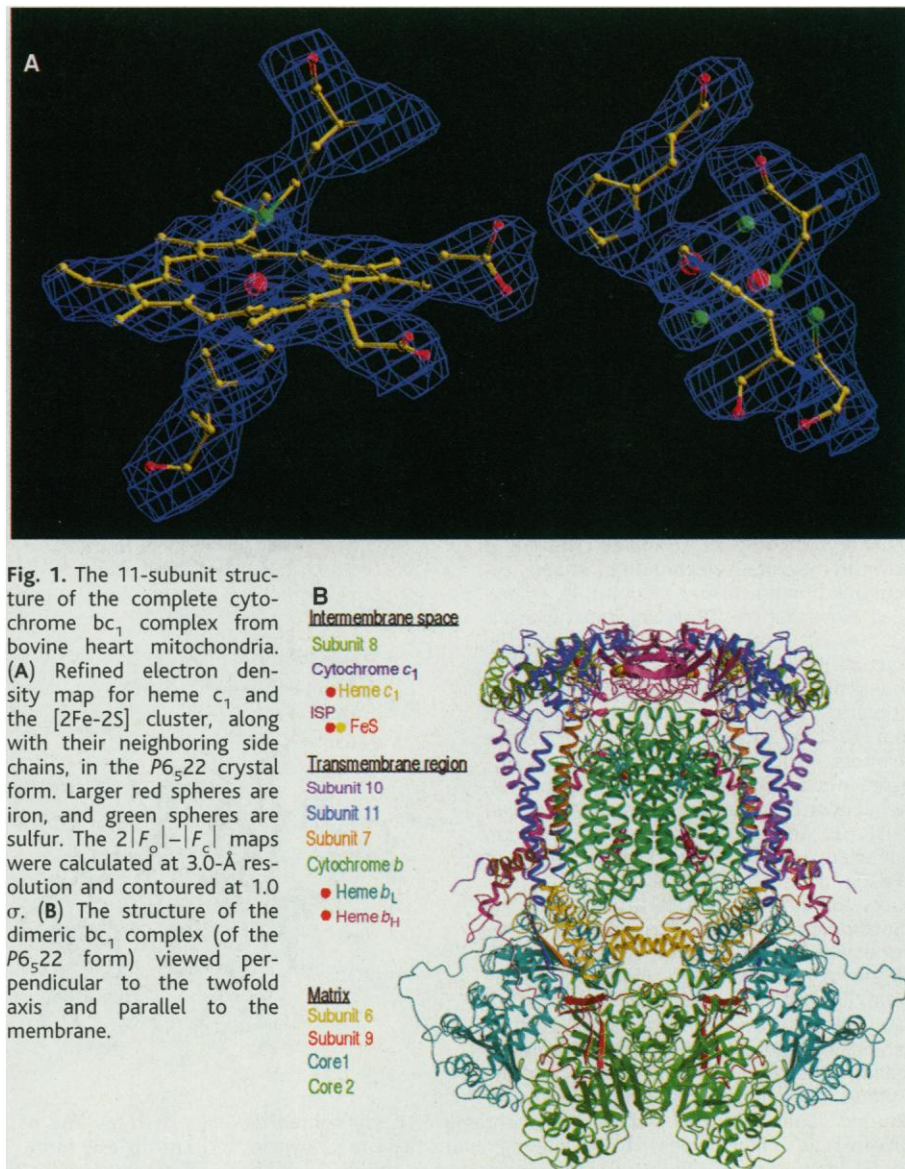


Fig. 1. The 11-subunit structure of the complete cytochrome bc_1 complex from bovine heart mitochondria. (A) Refined electron density map for heme c_1 and the [2Fe-2S] cluster, along with their neighboring side chains, in the $P6_522$ crystal form. Larger red spheres are iron, and green spheres are sulfur. The $2|F_o| - |F_c|$ maps were calculated at 3.0-Å resolution and contoured at 1.0 σ . (B) The structure of the dimeric bc_1 complex (of the $P6_522$ form) viewed perpendicular to the twofold axis and parallel to the membrane.

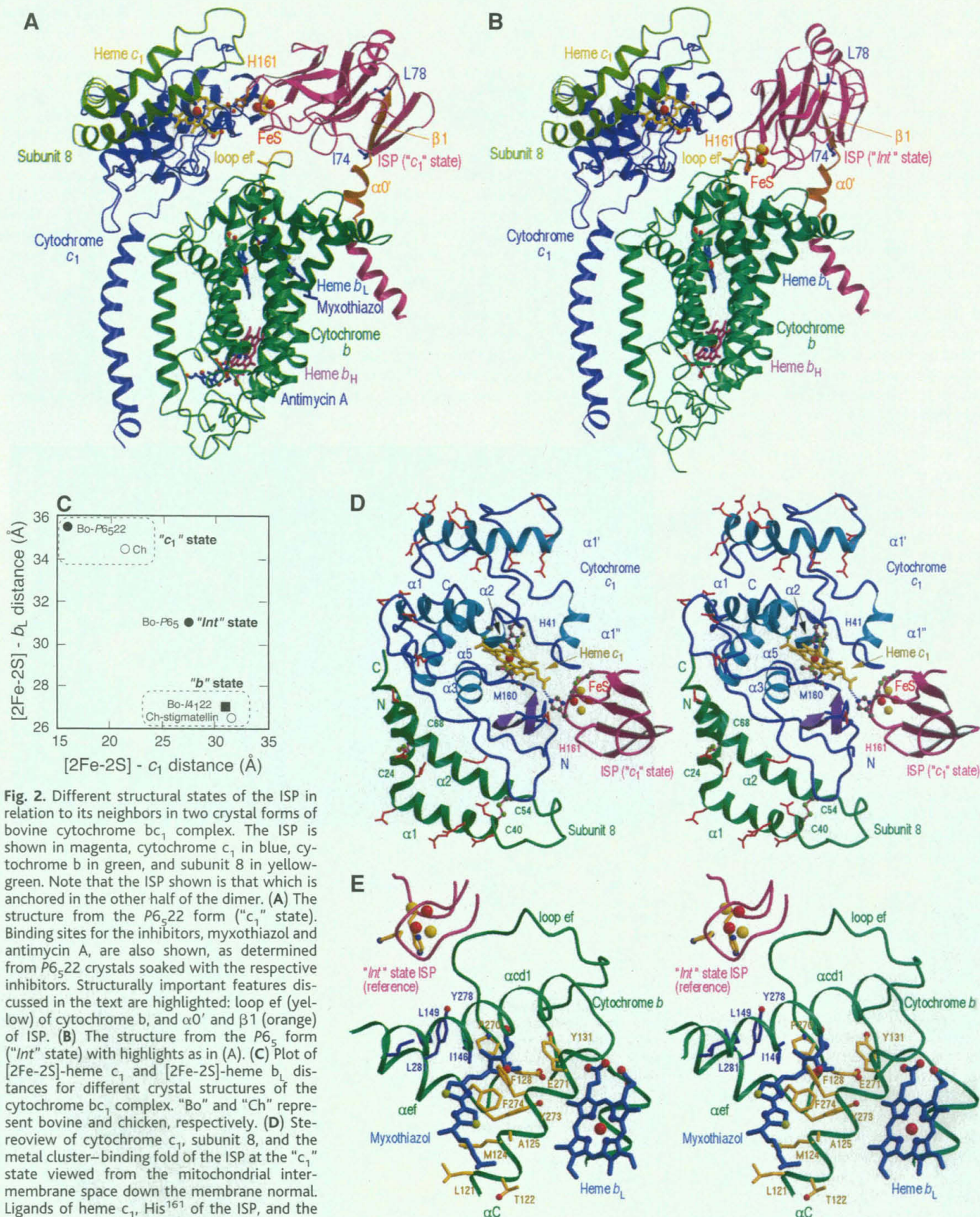


Fig. 2. Different structural states of the ISP in relation to its neighbors in two crystal forms of bovine cytochrome bc_1 complex. The ISP is shown in magenta, cytochrome c_1 in blue, cytochrome b in green, and subunit 8 in yellow-green. Note that the ISP shown is that which is anchored in the other half of the dimer. (A) The structure from the P6₅22 form ("c₁" state). Binding sites for the inhibitors, myxothiazol and antimycin A, are also shown, as determined from P6₅22 crystals soaked with the respective inhibitors. Structurally important features discussed in the text are highlighted: loop ef (yellow) of cytochrome b , and $\alpha 0'$ and $\beta 1$ (orange) of ISP. (B) The structure from the P6₅ form ("Int" state) with highlights as in (A). (C) Plot of [2Fe-2S]-heme c_1 and [2Fe-2S]-heme b_L distances for different crystal structures of the cytochrome bc_1 complex. "Bo" and "Ch" represent bovine and chicken, respectively. (D) Stereoview of cytochrome c_1 , subunit 8, and the metal cluster-binding fold of the ISP at the "c₁" state viewed from the mitochondrial intermembrane space down the membrane normal. Ligands of heme c_1 , His¹⁶¹ of the ISP, and the disulfide bonds in subunit 8 are shown. The distorted double-stranded β -sheet of cytochrome c_1 is highlighted in purple. Acidic residues exposed to the intermembrane space are shown in red. (E) Stereoview of the myxothiazol binding site in the P6₅22 form

("c₁" state). The position of the metal-binding cluster as determined from the P6₅ form ("Int" state) is added (upper left side), merely as a reference point for comparison.

(12). Loop $\alpha 1'$ - $\alpha 2$, together with $\beta 2$, form a docking site for the ISP in the $P6_322$ form.

Subunit 8—"acidic/hinge protein." Subunit 8 is sometimes referred to as the "hinge protein," because it is thought to be essential for proper complex formation between cytochromes c and c_1 (13). This subunit is also known as the "acidic protein," because it contains 24 acidic residues out of 78 total (13). It is composed of two long helices (helix $\alpha 1$, Pro¹⁶ to Arg⁴⁷, and helix $\alpha 2$, Cys⁵⁴ to Leu⁷⁷) connected by two disulfide bridges (Cys²⁴-Cys⁶⁸ and Cys⁴⁰-Cys⁵⁴), as expected from biochemical studies (Fig. 2D) (13). Both helices are kinked at Leu²⁷ and Lys⁷²; helix $\alpha 1$ is kinked by 90°, forming two separate helices. No electron density is observed for the NH₂-terminal 14 residues, which contain eight consecutive glutamic acids, suggesting that this segment may be highly mobile. The first visible residue on this NH₂-terminal portion is 22 Å away from heme c_1 , and the missing NH₂-terminal 14 residues may form a part of the cytochrome c docking site, together with helix $\alpha 1'$ and loop $\alpha 3$ - $\beta 1$ of cytochrome c_1 . Eight other acidic residues on helix $\alpha 1$ point into the solvent region on the same edge of heme c_1 (Fig. 2D) to form a large, negatively charged docking port for the highly basic cytochrome c .

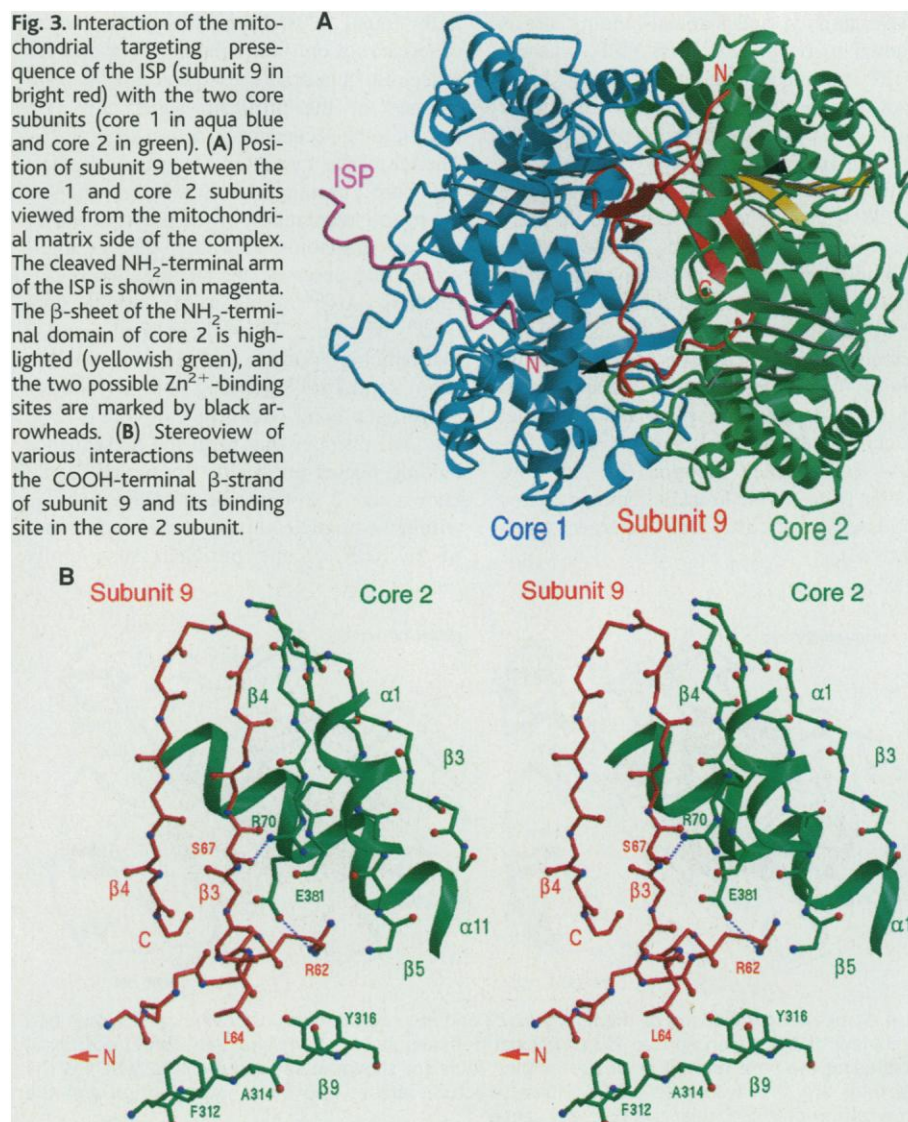
Transmembrane Region. Subunits 10 and 11. Subunits 10 and 11 both consist of single transmembrane helices with the NH₂-termini on the matrix side (Fig. 1B). These subunits maintain contact with cytochrome c_1 and the ISP (4), and have been implicated to play a role in the proper assembly of the bc_1 complex (14). Subunit 10 contains 62 residues and forms three helices: two short helices found at the NH₂- and COOH-terminal ends, in addition to a longer transmembrane helix in the middle (helix $\alpha 1$, residues 4 to 15; transmembrane helix $\alpha 2$, residues 17 to 48; helix $\alpha 3$, residues 51 to 56). Residues 4 to 31 of subunit 10 interact with both transmembrane helices of the ISP and cytochrome c_1 . The peripheral helix $\alpha 3$ also interacts with helices $\alpha 1$ and $\alpha 1'$ of cytochrome c_1 , which may explain the tight association observed between subunit 10 and cytochrome c_1 in dissociation experiments (4).

Subunit 11 has only one transmembrane helix (helix $\alpha 1$, residues 17 to 35), which interacts with the first half of the transmembrane helix of the ISP and subunit 10. Both NH₂ and COOH-terminal extensions are disordered. This subunit is peripherally located and is easily removed by delipidation without loss of activity (15). Helices $\alpha 2$ and $\alpha 3$ of subunit 10 together with the COOH-terminal extension of subunit 11 form a polar invagination. This invagination is located near the transmembrane helices of the ISP and cytochrome c_1 , as well as subunit 8 near the intermembrane side, and is large enough to accommodate the cluster-binding fold of the

ISP. This structural feature, therefore, might be related to the insertion of the [2Fe-2S] cluster into the ISP.

Inhibitor binding sites in cytochrome b . Cytochrome b has eight transmembrane helices (helices αA through αH) and four horizontal helices on the intermembrane side (helices αab , $\alpha cd1$, $\alpha cd2$, and αef). The two hemes, b_L and b_H , are in the center of a four- α -helical bundle formed by helices αA , αB , αC , and αD . Hemes b_L and b_H are close to the intermembrane and matrix sides, respectively. From inhibitor-soaked crystals, electron densities for myxothiazol and antimycin A are observed close to hemes b_L and b_H , respectively. Here, the structure of the myxothiazol binding site is described, because it will be relevant for the following discussion on the hydroquinone oxidation mechanism. Myxothiazol binds in the hydroquinone oxidation (Q_p) site of the bc_1 complex and blocks electron transfer to both the ISP and heme b_L (16). The binding site of the

inhibitor is underneath helix $\alpha cd1$ and is surrounded by helices αC , αF , and αef (8). In the current structure, the MOA group of myxothiazol is in the hydrophobic pocket formed by residues Pro²⁷⁰, Phe¹²⁸, Phe²⁷⁴, and Glu²⁷¹ (Fig. 2E). The methoxyacrylate group is within 8 Å of heme b_L , although there is no direct contact between the inhibitor and the heme. Electron transfer from the semiquinone (SQ^\bullet) to heme b_L could be mediated by hydrophobic residues, including Tyr¹³¹. At this position, the inhibitor is not accessible to the solvent, because the upper part of the cavity is blocked by residues from helix $\alpha cd1$ and loop ef . It is likely that in the process of hydroquinone oxidation, one histidine ligand of the [2Fe-2S] cluster forms a direct hydrogen bond with QH^- or SQ^\bullet (17). Therefore, an alternate quinone binding site is expected. Next to the current position of the MOA group, there is a hydrophobic hole that contacts the surface of the intermembrane side. This hole includes Ile¹⁴⁶, Leu²⁸¹, Leu¹⁴⁹, and



Tyr²⁷⁸ (Fig. 2E), and is the most likely alternate QH⁻ or SQ[•]-binding position when the quinone intermediate binds to the ISP.

Matrix Side. Subunit 9. Subunit 9 contains 78 amino acids and is the mitochondrial targeting presequence of the ISP (18). In eukaryotes, the ISP is nuclear coded and imported posttranslationally into the mitochondria, where it is inserted into the inner membrane (19). In mammals, the presequence is cleaved in a single step after the ISP is inserted in the bc₁ complex. In our structure, this presequence is found between the core 1 and core 2 subunits (Fig. 3A). The core 1 and core 2 subunits show high sequence homology to the general MPP, which cleaves targeting presequences after import into the mitochondria. These core proteins and MPPs belong to a family of Zn²⁺-dependent metalloendoproteases, which includes insulin-degrading enzymes from mammals and *Escherichia coli* pitrilysin (20). Mammalian MPPs are soluble heterodimers with an α and β subunit, and are located in the mitochondrial matrix. Both subunits are required for proteinase activity, and a metal-binding site is assumed to be present in β -MPP, whereas α -MPP is thought to be involved in the binding of the presequence because the precursor protein is cross-linked preferentially to it (21). The core 1 protein of bovine heart bc₁ complex shows higher sequence homology to β -MPP, whereas the core 2 protein is more closely related to α -MPP (6, 7). The location of subunit 9 close to the possible catalytic site suggests that it is cleaved directly from the ISP by these core proteins. Although isolated bovine heart bc₁ complexes lack processing activity, the core proteins constitute the general MPP function for plant mitochondrial bc₁ complexes that lack subunit 9 (7). Recently, it has been reported that the core proteins from bovine heart bc₁ complex show peptidase activity after mild detergent treatment (22).

Although subunit 9 has some contact with core 1, the binding site is predominantly on the core 2 protein (Fig. 3A). Subunit 9 is an extended peptide comprising two β -sheets, one at the COOH-terminal end and the other in the middle region. It is important to note that the COOH-terminal 15 amino acids form an extended β -sheet together with two β -strands of the NH₂-terminal domain of the core 2 subunit (Fig. 3B). The sequence of the last 17 COOH-terminal amino acids (residues 62 to 78) of subunit 9 is RPLVASVSLNVPASVRY (23), which contains a consensus motif (RX Φ XXS, where Φ is a hydrophobic amino acid) for interaction with MPP at positions -17, -15, and -12 relative to the cleavage site (18). Based on the determined structure at hand, the following two factors seem to be crucial elements responsible for the recognition of these 17 amino acids: (i) formation of the extended β -sheet together with the core 2 subunit, and (ii) the involvement of the consensus motif in specific interactions (Fig. 3B). Residues 64 to 76 are predominantly amino acids that are preferentially found in β -sheets; this preference is observed not only for subunit 9, but also for other mitochondrial presequences (24). Proteinases of the pitrilysin superfamily are known to be secondary-structure specific (6). Therefore, the formation of a shared β -sheet with core 2 protein is likely to be essential for the proper recognition of the presequence by the core 2 subunit. Secondly, specific interactions are observed for all three consensus residues: Arg⁶² forms a salt bridge with Glu³⁸¹ of core 2; Leu⁶⁴ is situated inside a hydrophobic pocket formed by Phe³¹², Ala³¹⁴, and Tyr³¹⁶ of core 2; and Ser⁶⁷ forms a hydrogen bond with Arg⁷⁰ of core 2 (Fig. 3B). All residues that form the presequence binding pocket are highly conserved for all known core 2 proteins and α -MPPs. Arg⁷⁰ is within the predicted inverse zinc-binding motif HXXEH of the pitrilysin superfamily

where only the first H is conserved and E in the fourth position is replaced by R/K/N in the core 2 subunits.

Although a clear binding site is observed for the presequence, the metal-binding site in the core subunits cannot be conclusively identified. This could be due to the EDTA treatment of the mitochondrial membrane in the purification of the enzyme. From the sequence alignment, an inverted zinc-binding motif (HXXEH-X₇₆-E) is predicted for MPP. However, neither core 1 nor the core 2 subunits contain the complete motif; in the core 1 subunit, the first His is replaced by Tyr, while for the core 2 subunit, the first His is the only conserved residue. Because the core 1 subunit is thought to be equivalent to β -MPP, this consensus sequence in the core 1 subunit is a candidate for the Zn²⁺-binding site. In our structure, Tyr⁵⁷, Glu⁶⁰, His⁶¹, and Glu¹³⁷ are found in close proximity; the arrangement of Tyr⁵⁷, His⁶¹, and Glu¹³⁷ appears suitable for a metal-binding site. However, in the current electron density map, only a weak electron density for a solvent molecule between His⁶¹ and Glu¹³⁷ is observed. Furthermore, metal ion density could not be observed in the region near the incomplete consensus sequence on the core 2 subunit, which contains His⁶⁷ and Asp¹⁴⁷ in close proximity.

The possible metal-binding sites described above are shown (Fig. 3A; arrowheads) together with the NH₂-terminus of the ISP. Both sites are distant from the COOH-terminus of subunit 9, which is located 25 and 15 Å away from the possible active sites in the core 1 and core 2 subunits, respectively; also, the COOH-terminus of subunit 9 is 30 Å away from the NH₂-terminus of the ISP. This indicates that a large structural rearrangement must occur after cleavage of the presequence.

Structural Changes at "Rieske" [2Fe-2S] Protein. In the P₆₅22 form, where the [2Fe-2S] cluster is in the "c₁" position, the functional domain of the ISP interacts with residues of the cytochrome c₁ subunit (loop α 1'- α 2, β 2, loop α 3- β 1, and heme c₁) as well as loop ef of cytochrome b (Fig. 2A). Most of these interactions are van der Waals contacts, and in the current structure only three hydrogen bonds, including one between His¹⁶¹ of the ISP, which is one of the ligands of the [2Fe-2S] cluster, and a propionate group of heme c₁ are observed (Fig. 2A). For the ISP, contact with other subunits mainly involves loops β 4- β 5 and β 6- β 7 in the cluster binding fold. All 127 C α positions from the high-resolution structure of the water-soluble "Rieske" fragment (25) can be superimposed onto the ISP at the "c₁" position with an rms difference of 0.93 Å. The main measurable difference is observed at strand β 1, where the functional domain is connected to the transmembrane anchor. This difference can easily

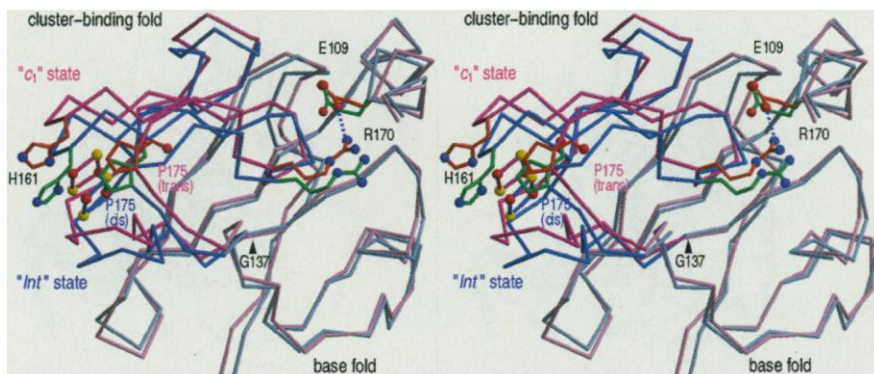


Fig. 4. Structural comparison of the ISP in P₆₅22 and P₆₅ crystal forms of bovine cytochrome bc₁. Stereoview of the superimposed ISP functional domains at "c₁" (red) and "Int" (blue) positional states using the base folds. The cluster-binding folds are shown in saturated colors, whereas the base folds are shown in pale colors. These structures are related by a hinge motion and the isomerization of Pro¹⁷⁵ near the [2Fe-2S] center.

be accounted for, because in the soluble fragment, the $\beta 1$ strand is free, while in the bc_1 complex, it is connected to the transmembrane helix. When the $\beta 1$ strand is omitted, the rms difference drops to 0.63 Å, which is comparable to the estimated average coordinate error of the structure (0.55 Å).

In the $P6_5$ form, where the [2Fe-2S] cluster is in the "Int" position, the binding site for the functional domain of the ISP is formed by residues in loop ef, loop gh, and a short loop between helices $\alpha cd 2$ and helix αd of cytochrome b (Fig. 2B). No interaction between the [2Fe-2S] cluster of the ISP and cytochrome c_1 is observed. Most of the interactions are van der Waals contacts, except for a clear hydrogen bond between Lys⁹⁰N_ε of the ISP and Asp¹⁷¹O_{δ2} of cytochrome b. Extensive contacts exist between loop ef and the ISP, and it is loop ef that shows the largest structural difference between our two forms of cytochrome b. The average displacement for cytochrome b residues 262 to 267 is 1.1 Å, and the largest displacement is observed for residues Thr²⁶⁴ and Pro²⁶⁵. Notably, Pro²⁶⁵ is conserved in all known cytochrome b sequences. The contact region on the ISP is formed by loops $\beta 4$ - $\beta 5$ and $\beta 6$ - $\beta 7$, and a β -turn region between $\beta 2$ and $\beta 3$.

The structural differences in the ISP found between the $P6_5$ and $P6_5$ crystal forms can be attributed to two prominent alterations (Fig. 4): (i) rotation of the entire functional domain; and (ii) displacement of the metal cluster binding fold relative to the base fold within the functional domain. The rotation of the entire functional domain is approximately a 35° rotation around the pivot point (Ile⁷⁴) near the COOH-terminal end of the short helix $\alpha 0'$ (Fig. 2, A and B). A hydrogen bond Leu⁶⁹O-Ser⁷²N is present in the " c_1 " form, which induces a 3_{10} -helix conformation, but not in the "Int" form, where the 3_{10} -helix is absent. An additional structural difference is observed within strand $\beta 1$ where Leu⁷⁸ for the "Int" form is buried in the protein, whereas in the " c_1 " form, it is exposed to the solvent. This transition alone contributes only 6° to the rotation of the subunit.

Conformational differences within the functional domain are rather small but are nevertheless significant. The functional domain of the ISP has two separate folds or subdomains (Fig. 4): the metal cluster binding fold (residues 137 to 181) and the base fold (residues 74 to 136 and 182 to 196) (25). Clear positional displacement between these two folds is observed between the "Int" and " c_1 " forms. As mentioned above, the structure of the ISP subunit at the " c_1 " position is the same as that of the water soluble ISP fragment. However, at the "Int" position, the cluster-binding fold appears to be detached from the base fold in an "open" conformation. If the functional domains of the two

crystal forms are superimposed using the base fold residues, the rms difference of the $C\alpha$ positions of the cluster fold is 1.6 Å. In the "Int" form, the salt bridge Glu¹⁰⁹-Arg¹⁷⁰ as well as the associated hydrogen bond network between the cluster binding fold and the base fold, which connects these two structures in the " c_1 " form, are absent (Fig. 4). As a result, the gap between the two folds becomes exposed to the solvent. In addition, Pro¹⁷⁵ in the "Int" form is best fitted with a *cis*-proline instead of the *trans*-proline that is observed in the " c_1 " form and in the structure of the water-soluble ISP fragment.

This conformational change is represented by a hinge motion of the cluster-binding fold. A conformational change between the two forms also occurs within the following two loops: at one end of the metal cluster binding fold where Gly¹³⁷ shows a slight bend in the strand and at the other end where Pro¹⁷⁵ shows the *cis*["Int"]/*trans*[" c_1 "] transition. As a result of this conformational change, the cluster-binding fold rotates by approximately 6° around a position close to Gly¹³⁷. This rotation causes a 2-Å displacement for the position of the [2Fe-2S] cluster. It should be noted that *cis*-Pro¹⁷⁵ is also found in the structure of the water soluble "Rieske" fragment from the b_6f complex, which is a counterpart of the bc_1 complex in chloroplasts (26). Remarkably, the relative position between the cluster binding and base

folds in our "Int" form shows greater similarity to the structure of the soluble b_6f ISP fragment than to the ISP found in our " c_1 " form. When the structure of the ISP in the " c_1 " form and that of the soluble b_6f ISP fragment are superimposed on the "Int" structure using the common base fold residues ($\beta 2$ and $\beta 3$), the rms difference of the $C\alpha$ atoms in the cluster-binding fold is 1.6 Å for the " c_1 " form and 1.0 Å for the b_6f ISP fragment. This suggests that the structural differences within the ISP subunits described above may be intimately related to the mechanism of bc_1 and b_6f complexes.

Possible Mechanism of Hydroquinone Oxidation. It is generally accepted that electron transfer is coupled to proton translocation by the protonmotive Q-cycle mechanism first proposed by Mitchell (1). The central reaction of the Q-cycle is a bifurcation of the electron pathway upon oxidation of hydroquinone at the Q_p site that is in contact with the positive side (intermembrane side) of the membrane (27). During the hydroquinone oxidation reaction, one electron is transferred via the "high-potential chain" (ISP's [2Fe-2S] cluster and cytochrome c_1) to cytochrome c , while the second electron is transferred to heme b_L and from there, across the membrane dielectric to heme b_H [recent reviews in 2, 17, 28)]. Heme b_H is a part of the quinone reduction (Q_N) site which is in contact with the negative side (matrix side) of the mem-

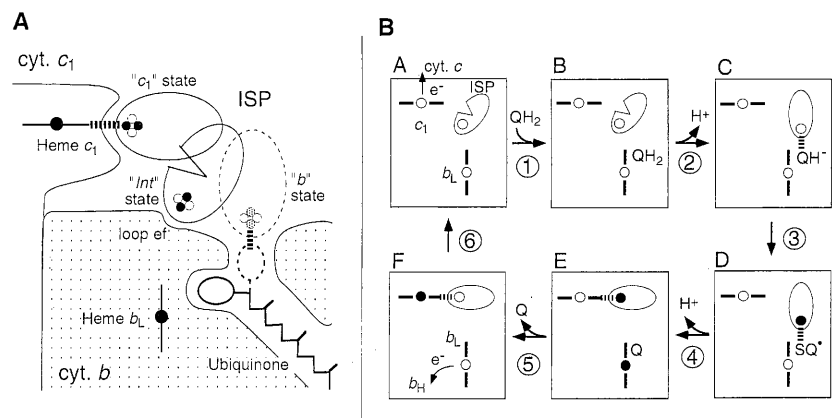


Fig. 5. (A) A schematic drawing of the different positional states of the ISP functional domain. The " c_1 ", "Int", and "b" states of the ISP functional domain are shown. Thick dashed lines indicate hydrogen bonds formed by the [2Fe-2S] cluster. The difference in the oval shape between the " c_1 " and "Int" positions represent the conformational change occurring within the ISP functional domain. The ISP at the "b" position is shown in a dotted line because its protein conformation has not yet been revealed for the bovine bc_1 complex. With the ISP at the "b" position, the head group of the bound ubiquinone takes a conformation shown in the dotted lines to form hydrogen bonds with the ISP. **(B)** Proposed mechanistic model of hydroquinone oxidation at the Q_p site of the bc_1 complex based on the switching of the ISP between the "Int" position (A and B), the "b" position (C and D), and the " c_1 " position (E and F). The oxidized [2Fe-2S] cluster is shown in the resting, "Int" state (A). Hydroquinone (QH₂) binds (step 1) and must first be deprotonated (step 2) before it can interact with the [2Fe-2S] cluster (C). After the first electron transfer from QH₂ to the [2Fe-2S] cluster (step 3), the resulting semiquinone (SQ•) is stabilized by the ISP in the "b" positional state (D). After the second electron transfer (step 4), the reduced ISP switches to the " c_1 " positional state since ISP can not form a hydrogen bond with oxidized Q, and transfers its electron to cytochrome c_1 (step 5). Electrons are transferred to cytochrome c and heme b_L , respectively, and the oxidized ISP reverts to its "Int" positional state (step 6). Filled circles are reduced centers, empty circles are oxidized centers. Thick dashed lines indicate hydrogen bonds formed by the [2Fe-2S] cluster. For details, see text.

brane; at the Q_N site, heme b_H reduces quinone to hydroquinone. The antimycin inhibitor binds at this Q_N site (Fig. 2A).

Several mechanisms have been suggested to explain this bifurcation of the electron flow (29–31). Brandt and von Jagow have proposed two different conformational states and a “catalytic switch” mechanism (30, 31). This was supported by earlier structures of the bc_1 complex that suggest two different locations for the functional domain of the ISP (9). The transition between the two states has been described as a passive diffusion between two docking sites on cytochrome c_1 and cytochrome b_L . However, the structural evidence we present, along with previous biochemical data, favor a “three state” model over a “two state” model for the following reasons (Fig. 5): (i) Studies of the ISP within the bc_1 complex suggest that the oxidized [2Fe-2S] cluster is not involved in hydrogen bonding in the bc_1 complex (32). The “*Int*” positional state as seen in the $P6_5$ crystals most likely represents this oxidized state, where the [2Fe-2S] cluster is sufficiently far away from cytochrome c_1 and cytochrome b_L to prohibit hydrogen bonding. (ii) Stigmatellin, which

mimics the quinone intermediate, binds to cytochrome b_L and the reduced ISP (33). A direct interaction of stigmatellin with both cytochrome b_L and the [2Fe-2S] cluster is reported in the chicken bc_1 complex structure when the ISP is in the “b” positional state (9). Thus, the reduced ISP should occupy the “b” positional state when the reduced [2Fe-2S] cluster interacts with QH^- or SQ^\bullet . (iii) When the [2Fe-2S] cluster is oxidized, a weak interaction with myxothiazol bound in the vicinity of heme b_L is observed, while no interaction is observed when the [2Fe-2S] cluster is reduced (31). This suggests that the reduced [2Fe-2S] cluster occupies the “ c_1 ” positional state preferentially when QH^- or SQ^\bullet is not present in the Q_P site.

Using the new “three state” model, hydroquinone oxidation reaction can be readily explained as follows (Fig. 5). When the complex is fully oxidized and before any hydroquinone is bound, the ISP is in the “*Int*” positional state (Fig. 5B; A). Hydroquinone will bind in the quinone-binding site formed by the end of helix αC , helix $\alpha d1$ and loop ef of cytochrome b (Fig. 2E and Fig. 5B; B). Before hydroquinone can

be oxidized, it must first be deprotonated (step 2); this deprotonation represents the activation barrier of hydroquinone oxidation (34). The interaction with the deprotonated hydroquinone (QH^-) will move the ISP toward the “b” positional state (Fig. 5B; C). After the electron transfer (step 3), the resulting semiquinone is tightly bound to the reduced [2Fe-2S] cluster in the “b” positional state (Fig. 5B; D); in this state, the semiquinone intermediate will be stabilized (17). After the second electron transfer from semiquinone to heme b_L (step 4), the interaction between the [2Fe-2S] cluster and the resulting quinone is weakened so that the reduced ISP can now occupy the preferred “ c_1 ” positional state (Fig. 5B; E) which allows rapid electron transfer from the [2Fe-2S] cluster to heme c_1 (step 5). Finally, when the electrons have been transferred to cytochrome c and to heme b_H , the ISP can go back to its initial “*Int*” positional state (step 6), and the site is ready for the next reaction cycle. All electron transfer reactions occur between species when they are hydrogen bonded to each other; therefore, electron transfer will

Table 1. Summary of x-ray data collection and MIR phase determination. X-ray data used for this structure determination were collected at ID2/BL4 and ID14/EH3 at ESRF. Intensity data were obtained using Mar IP detectors (ID2/BL4) or Mar CCD detector (ID14/EH3). Data were processed with DENZO and SCALEPACK (35). Initial phases were obtained for the $P6_522$ crystals by multiple isomorphous replacement (MIR). MIR phasing and refinement of the heavy atom positions were carried out using the program MLPHARE (36). MIR phases were calculated up to 4.0-Å resolution. The overall figure of merit was 0.51. Density modification and phase extension to 3.0-Å for the $P6_522$ crystal form was performed with the program DM (37). The initial free- R factor was 0.524 and was reduced to 0.268 after 200 cycles. The best result was obtained with a solvent content of 64%. Using this electron density, the structure of the $P6_5$ crystal form was solved using the program AMORE (38). Multicrystal averaging between two crystal forms was performed using the program DMMULTI (37), after which the

free- R factor for the $P6_522$ and $P6_5$ forms were 47% and 33%, respectively. Atomic models of the bc_1 complex were built using the program O (39). In the initial electron density map, the electron density for the ISP for both crystal forms was ambiguous. The density for the ISP appeared in different positions in the different crystal forms after the first cycle of refinement. Simulated annealing (β -test version of CNS; A. Brünger, personal communication) followed by positional refinement using the program REFMAC (40) resulted in a structural model with an R -factor of 28.5% and 32.0% for $P6_522$ and $P6_5$ forms, respectively, for the data between 30- and 3.0-Å resolution. The free R -factor within the same resolution range was 34.5% and 36.5% for $P6_522$ and $P6_5$ forms, respectively (from 2% of the data). The rms deviations from standard values of bond lengths and angles for $P6_522$ and $P6_5$ forms were 0.012 Å and 3.4°, 0.013 Å and 3.6°, respectively. All the figures here were created using the programs O (39), MOLSCRIPT (41), and RASTER3D (41).

Crystal	d_{min} (Å)	Observations		Completeness (%)	R_{merge}^* (%)	R_{deriv}^\dagger (%)	Sites (n)	R_c^\ddagger	Station
		Overall	Unique						
<i>Diffraction Data</i>									
<i>P6₅₂₂ form</i>									
Native (initial phasing)	4.0	89,521	32,694	84.0	5.5	—	—	—	ID14
(Me) ₃ PbAc (24 hour)	4.0	81,641	31,025	77.7	9.8	13.9	3	0.83	ID2
(Me) ₃ PbAc (48 hour)	4.0	65,722	27,344	69.3	7.8	11.1	3	0.84	ID2
EMTS (12 hour)	4.0	97,696	33,871	85.4	9.1	15.9	11	0.82	ID2
EMTS (18 hour)	4.0	82,477	31,153	79.3	9.1	15.8	11	0.76	ID2
EMTS (co-crystallized)	4.0	34,150	18,976	48.2	4.5	11.2	7	0.87	ID14
Native (high resolution)	3.0	223,182	79,396	88.9	7.0	—	—	—	ID2
Myxothiazol	3.0	172,070	71,966	77.2	9.4	—	—	—	ID2
Antimycin A	3.3	138,911	55,170	79.0	10.5	—	—	—	ID2
<i>P6₅ form</i>									
Native	3.0	440,419	111,672	81.9	9.2	—	—	—	ID2

<i>MIR Phase Determination</i>									
Resolution (Å)	19.1	10.8	7.5	5.8	4.7	4.0			
Reflections	215	1591	3514	4990	5293	2535			
Figure of merit	0.44	0.54	0.52	0.57	0.50	0.39			

* $R_{merge} = \sum_i \sum_h |I_i(h) - \langle I(h) \rangle| / \sum_i \sum_h I_i(h)$, where $I_i(h)$ is the i th measurement. $\dagger R_{deriv} = \sum |F_{PH} - |F_P|| / \sum |F_P|$, where F_{PH} and F_P are protein and heavy-atom derivative structure factors, respectively. $\ddagger R_c = \sum |F_{PH} - F_P| - F_{H(calc)}| / \sum |F_{PH} - F_P|$, F_{PH} and F_P are defined above, $F_{H(calc)}$ is the calculated heavy-atom structure factor. Summation is done using centric reflections only.

be extremely rapid and most likely not be rate limiting. The reaction rate is limited by the ubihydroquinone deprotonation reaction (34) and by the stability of the semiquinone intermediate (17).

References and Notes

1. P. Mitchell, *J. Theor. Biol.* **62**, 327 (1976).
2. U. Brandt and B. Trumpower, *Crit. Rev. Biochem. Mol. Biol.* **29**, 165 (1994).
3. D. E. Robertson *et al.*, *Biochemistry* **32**, 1310 (1993); X. H. Yang and B. L. Trumpower, *J. Biol. Chem.* **261**, 12282 (1986).
4. H. Schägger, T. A. Link, W. D. Engel, G. von Jagow, *Methods Enzymol.* **126**, 224 (1986).
5. H. Schägger, U. Brandt, S. Gencic, G. von Jagow, *ibid.* **260**, 82 (1995).
6. H.-P. Braun and U. K. Schmitz, *Trends Biochem. Sci.* **20**, 171 (1995).
7. H. P. Braun, M. Emmermann, V. Kruft, U. K. Schmitz, *EMBO J.* **11**, 3219 (1992).
8. D. Xia *et al.*, *Science* **277**, 60 (1997).
9. Z. Zhang *et al.*, *Nature* **392**, 677 (1998); A. R. Crofts *et al.*, *The Phototrophic Prokaryotes*, in *Proceedings of the IXth International Symposium on Phototrophic Prokaryotes*, 6 to 12 September 1997, Vienna, G. A. Peschek, W. Loeffelhardt, G. Schmetterer, Eds. (Plenum, New York, in press).
10. The $P6_522$ crystal form was prepared as previously described [E. A. Berry, L. Huang, T. N. Earnest, B. K. Jap, *J. Mol. Biol.* **224**, 1161 (1992)]. In short, crystals were obtained using 0.015% *n*-dodecyl- β -D-maltoside (DDM), 100 mM NaCl, and 6 to 8% PEG4000. The resolution of these crystals was effectively enhanced from 3.8 Å to 3.0 Å by dehydration using a heavy metal compound. The $P6_5$ form was crystallized under similar conditions as for $P6_522$ crystals, except that a mixture of DDM and HECAMEG was used as detergent and the pH was slightly higher (pH 7.2). Size of the hexagonal bipyramidal shaped crystals of the $P6_522$ form ranged from 0.1 to 0.8 mm on edge, while the hexagonal rod-shaped $P6_5$ forms were typically 0.1 to 0.3 mm thick and 1 to 4 mm long. Flash-cooling was performed on these x-ray-sensitive crystals so that an entire data set could be collected from a single crystal [J. W. Lee, M. Chan, T. V. Law, H. J. Kwon, B. K. Jap, *J. Mol. Biol.* **252**, 15 (1995)].
11. R. P. Ambler, in *From Cyclotrons To Cytochromes*, N. O. Kaplan and A. Robinson, Eds. (Academic Press, New York, 1982), pp. 263–280.
12. J. Stonehuerner *et al.*, *J. Biol. Chem.* **260**, 5392 (1985).
13. C. H. Kim and T. E. King, *ibid.* **258**, 13543 (1983); S. Wakabayashi, H. Takeda, H. Matsubara, C. H. Kim, T. E. King, *J. Biochem.* **91**, 2077 (1982); K. Mukai, T. Miyazaki, S. Wakabayashi, S. Kuramitsu, H. Matsubara, *ibid.* **98**, 1417 (1985).
14. J. D. Phillips, L. A. Graham, B. L. Trumpower, *J. Biol. Chem.* **268**, 11727 (1993).
15. H. Schägger *et al.*, *Eur. J. Biochem.* **190**, 123 (1990).
16. G. von Jagow and T. A. Link, *Methods Enzymol.* **126**, 253 (1986).
17. T. A. Link, *FEBS Lett.* **412**, 257 (1997).
18. U. Brandt, L. Yu, C.-A. Yu, B. L. Trumpower, *J. Biol. Chem.* **268**, 8387 (1993).
19. F. U. Hartl and W. Neupert, *Science* **247**, 930 (1990); B. S. Glick, E. M. Beasley, G. Schatz, *Trends Biochem. Sci.* **17**, 453 (1992).
20. N. D. Rawlings and A. J. Barrett, *Biochem. J.* **290**, 205 (1993).
21. V. Pačes, L. E. Rosenberg, W. A. Fenton, F. Kalousek, *Proc. Natl. Acad. Sci. U.S.A.* **90**, 5355 (1993); M. Arretz, H. Schneider, B. Guiard, M. Brunner, W. Neupert, *J. Biol. Chem.* **269**, 4959 (1994); M. J. Yang *et al.*, *ibid.* **266**, 6416 (1991).
22. K. Deng *et al.*, *Biophys J.* **72**, 319a (1996).
23. Single-letter abbreviations for the amino acid residues are as follows: A, Ala; C, Cys; D, Asp; E, Glu; F, Phe; G, Gly; H, His; I, Ile; K, Lys; L, Leu; M, Met; N, Asn; P, Pro; Q, Gln; R, Arg; S, Ser; T, Thr; V, Val; W, Trp; and Y, Tyr. X indicates any residue.
24. J. P. Hendrick, P. E. Hodges, L. E. Rosenberg, *Proc. Natl. Acad. Sci. U.S.A.* **86**, 4056 (1989).
25. S. Iwata, M. Saynovits, T. A. Link, H. Michel, *Structure* **4**, 567 (1996).
26. C. J. Carrell, H. Zhang, W. A. Cramer, J. L. Smith, *ibid.* **5**, 1613 (1997).
27. M. K. Wikstrom and J. A. Berden, *Biochim. Biophys. Acta*, **283**, 403 (1972).
28. B. L. Trumpower, *J. Biol. Chem.* **265**, 11409 (1990); U. Brandt, *FEBS Lett.* **387**, 1 (1996); *Biochim. Biophys. Acta* **1365**, 261 (1998).
29. A. R. Crofts and Z. Wang, *Photosynth. Res.* **22**, 69 (1989); H. Ding *et al.*, *Biochemistry* **34**, 15979 (1995).
30. U. Brandt and G. von Jagow, *Eur. J. Biochem.* **195**, 163 (1991).
31. U. Brandt, U. Haase, H. Schägger, G. von Jagow, *J. Biol. Chem.* **266**, 19958 (1991).
32. T. A. Link, O. M. Hatzfeld, M. Saynovits, in *Bioinorganic Chemistry. Transition Metals in Biology and their Coordination Chemistry*, A. X. Trautwein, Ed. (Wiley-VCH, Weinheim, Germany, 1997), pp. 312–325.
33. C. R. D. Lancaster and H. Michel, *Structure* **5**, 1339 (1997); G. von Jagow and T. Ohnishi, *FEBS Lett.* **185**, 311 (1985); D. E. Robertson, F. Daldal, P. L. Dutton, *Biochemistry* **29**, 11249 (1990).
34. U. Brandt and J. Okun, *Biochemistry* **36**, 11234 (1997).
35. Z. Otwinowski, in *Data Collection and Processing*, L. Sawyer, N. Isaacs, S. Bailey, Eds. (SERC Daresbury Laboratory, Warrington, UK, 1993), pp. 56–62.
36. Z. Otwinowski, in *Isomorphous Replacement and Anomalous Scattering*, W. Wolf, P. R. Evans, A. G. W. Leslie, Eds. (SERC Daresbury Laboratory, Warrington, UK, 1991), pp. 80–86.
37. K. D. Cowtan, *Joint CCP4 ESF-EACBM Newsl. Protein Crystallogr.* **31**, 34 (1994).
38. J. Navaza, *Acta Crystallogr. A* **50**, 157 (1994).
39. T. A. Jones, J. Y. Zou, S. W. Cowan, M. Kjeldgaard, *ibid.* **47**, 110 (1991).
40. G. N. Murshudov, A. A. Vagin, E. J. Dodson, *Acta Crystallogr. D* **53**, 240 (1997).
41. P. J. Kraulis, *J. Appl. Crystallogr.* **24**, 946 (1991); E. A. Merritt and M. E. P. Murphy, *Acta Crystallogr. D* **50**, 869 (1994).
42. Supported by funding from the Office of Health and Environmental Research, U.S. Department of Energy under contract DE-AC03-76SF00098 (B.K.J.); an appointment to the Alexander Hollaender Distinguished Postdoctoral Fellowship Program sponsored by the U.S. Department of Energy (Office of Health and Environmental Research) and administered by the Oak Ridge Institute for Science and Education (J.W.L.); the Swedish Research Councils, NFR and MFR (S.I.); a European Commission Biotechnology grant (S.I.); and the Wenner-Gren foundation (K.O.). Preliminary data collection and screening for heavy-atom derivatives were conducted at the following beamlines: Beamlines X4A, X12C, and X25 at National Synchrotron Light Source; beamlines 1-5 and 7-1 at Stanford Synchrotron Radiation Laboratory; and beamlines 6A, 6B, and 18B at the Photon Factory. The data collection at ID14 at European Synchrotron Radiation Facility was performed with the support of S. Wakatsuki, W. Burmeister, and T. Tomizaki. We sincerely thank all the staff members of these synchrotron facilities for their valuable assistance and for providing much-needed beamtime; J. Hajdu and P. Walian for useful discussions and reading of manuscripts; N. Chan and M. Chan for protein purification and crystallization; and D. Voges, J. Abramson, and S. Törnroth for data collection and processing. The coordinates are deposited in the Brookhaven Protein Data Bank [1BE3 ($P6_522$) and 1BGY ($P6_5$)].

3 April 1998; accepted 28 May 1998